Large Scale CVD Synthesis of Single-Walled Carbon Nanotubes

Alan M. Cassell,[†,‡] Jeffrey A. Raymakers,[†] Jing Kong,[†] and Hongjie Dai*[,†]

Department of Chemistry, Stanford University, Stanford, California 94305, and National Aeronautics and Space Administration, Ames Research Center, Moffett Field, California 94035

Received: March 18, 1999; In Final Form: June 1, 1999

The synthesis of bulk amounts of high quality single-walled carbon nanotubes (SWNTs) is accomplished by optimizing the chemical compositions and textural properties of the catalyst material used in the chemical vapor deposition (CVD) of methane. A series of catalysts are derived by systematically varying the catalytic metal compounds and support materials. The optimized catalysts consist of Fe/Mo bimetallic species supported on a novel silica−alumina multicomponent material. The high SWNT yielding catalyst exhibits high surface-area and large mesopore volume at elevated temperatures. Gram quantities of SWNT materials have been synthesized in ∼0.5 h using the optimized catalyst material. The nanotube material consists of individual and bundled SWNTs that are free of defects and amorphous carbon coating. This work represents a step forward toward obtaining kilogram scale perfect SWNT materials via simple CVD routes.

1. Introduction

Since Iijima's discovery of carbon nanotubes in arc-discharge soot materials,[1] nanotubes have generated significant research activities in chemistry, condensed matter physics, and materials science. Nanotubes are intriguing one dimensional systems ideally suited for fundamental studies of atomically well-defined materials and have high potential for technological applications.[2−4] Nanotubes exhibit the highest Young's modulus and tensile strength among all materials. A single-walled nanotube can be either metallic, semiconducting, or semimetallic depending on the helicity and diameter.[2] On the practical side, promising applications of nanotubes have been demonstrated including advanced scanning probes,[5−7] chemical force sensors,[8] electron field emission sources,[9−13] and nano-electronic components.[14−16]

High quality nanotube materials are desired for both fundamental and technological applications. High quality refers to the absence of structural and chemical defects over a significant length scale (e.g., 1−10 microns) along the tube axes. So far, arc-discharge[17,18] and laser-ablation[19] are the principal methods for obtaining high quality nanotube materials. However, there are several key issues concerning both methods. The first is that both methods involve evaporating carbon atoms from solid carbon sources at ≥3000 °C. This sets a limitation to the quantity of nanotubes that can be synthesized, and it has been unclear how to scale-up nanotube production to the kilogram level using evaporation approaches. The second issue relates to the fact that evaporation methods grow nanotubes in highly tangled forms mixed with unwanted forms of carbon or metal species. The nanotubes are difficult to purify, manipulate, and assemble for building nanotube device architectures. New synthetic strategies should open new possibilities in nanotube science and technology if exquisite control over their growth can be gained. The ultimate goal in nanotube synthesis should be gaining control over geometrical aspects of nanotubes, such as location and orientation, and the atomic structure of nanotubes including helicity and diameter. Moreover, such controlled synthesis must be scaled up in bulk or on surfaces.

Chemical vapor deposition of hydrocarbons over metal catalysts has been a classical method to produce carbon materials. Various forms of carbon fibers, filaments, and multiwalled nanotubes have been synthesized by CVD in the past.[20−24] However, previous CVD approaches mostly obtain defective tubular materials. Recently, we developed for the first time a CVD synthesis approach to high quality SWNTs by using methane as the carbon feedstock.[25,26] The choice of methane over other hydrocarbons was essential and based on its high stability at elevated temperatures (∼1000 °C), which virtually eliminates hydrocarbon self-pyrolysis that may lead to the generation of amorphous carbon and cause catalyst poisoning. We further developed a synthetic strategy using methane CVD on catalytically patterned substrates to obtain "nanotube chips" containing isolated single-walled nanotubes at controlled locations.[26] Integrated nanotube circuits were built in combination with microfabrication techniques, which reliably led to a large number of ohmically contacted nanotube devices with controllable length. Both metallic and semiconducting individual nanotubes have been observed in recent transport measurements. Transport studies demonstrated ohmic contacts to ∼5 μm long individual SWNTs, giving two-terminal resistances as low as 20 kΩ, even at 4.2 K.[16]

The current work focuses on the synthesis of bulk quantities of high quality SWNTs using the methane CVD approach. Noteworthy is that more recently, SWNTs have also been synthesized in bulk by CVD of benzene,[27] ethylene,[28] or a methane/hydrogen mixture.[29] In our initial bulk synthesis, the yield of SWNTs was not high.[25] However, we learned several important aspects of high quality SWNT growth using CVD. First, the type of support material for the catalyst was found to play a key role in the type of SWNTs produced. The Al_2O_3 supported Fe_2O_3 catalyst afforded a large fraction of individual SWNTs when subjected to methane CVD at 900−1000 °C, whereas silica supported Fe_2O_3 catalyst led to ropelike bundles of SWNTs.[25] This strongly suggested that a systematic investigation of various support materials may lead to the optimum

* To whom correspondence should be addressed.
† Department of Chemistry.
‡ NASA Ames Research Center.

10.1021/jp990957s CCC: $18.00
Published on Web 07/20/1999

catalyst for high yield SWNT production. Second, we found that base-growth is the dominant growth mechanism for SWNTs in the CVD process. That is, a significant amount of the ~1 nm scale metal catalyst particles (responsible for nucleating SWNTs) remained anchored on the catalyst support surface during the growth of nanotubes.[25] This result hinted that optimization of metal−support interactions should be pursued for higher yield and purity SWNTs.

Based on our previous results and understanding of the methane CVD process, we have carried out a step-by-step optimization of bulk SWNT growth. We have focused on investigating a series of catalyst materials prepared by systematically varying the metal composition and the support. The highest yield of SWNTs was achieved with an Fe/Mo bimetallic catalyst supported on a new type of $Al_2O_3-SiO_2$ hybrid material. We found that, in the CVD growth of nanotubes, the active metal catalytic species, metal−support interactions, resistance of the catalyst to sintering and the chemical, and physical nature of the support dictate the yield, purity, and quality of the nanotubes.

2. Experimental Section

Materials and Reagents. The main support material used in this work was the Oxide C alumina obtained from Degussa Inc. The material consists of crystalline transition alumina ($\gamma-\delta$ phase) nanoparticles and has a surface area of ~100 m^2/g. Tetraelthyl orthosilicate (TEOS), $(NH_4)_6Mo_7O_{24}\cdot 4H_2O$, $Fe_2(SO_4)_3\cdot 5H_2O$, $Fe(NO_3)_3\cdot 9H_2O$, and $Ru(acac)_3$ were purchased from Aldrich Chemical. Hydrofluoric acid and deionized water were supplied by J. T. Baker, Inc. Ethanol was purchased from Gold Shield Chemical Co. Pyridine and 1,2-dichloroethane were purchased from E. M. Science. Methane (99.99%) and Ar were supplied by Praxair, Inc.

Preparation of a $Al_2O_3-SiO_2$ Support Material. An $Al_2O_3-SiO_2$ multicomponent (hybrid) support was synthesized by forming silica sol in the presence of alumina nanoparticles and gelling the subsequent mixture. First, 1.0 g of alumina nanoparticles was suspended in 50 mL of ethanol with vigorous stirring. TEOS (2.2 mL) was introduced into the alumina suspension via syringe and allowed to stir for 10 min. Water (5 mL) was then added to hydrolyze the TEOS and form a silica sol mixed with alumina nanoparticles. Concentrated HF (0.47 mL, 28.9 M) solution was added 5 min later to catalyze the gelation of the silica sol. After 1 h, the suspension was heated to 90 °C, and a stream of N_2 was flown over the samples to evaporate the water and ethanol. The dried fluffy white powder was then carefully ground with an agate mortar, which affords the final $Al_2O_3-SiO_2$ hybrid support material. The molar ratios of the compounds involved in making the hybrid support are $TEOS:Al_2O_3:HF:H_2O:EtOH = 1:1:1.4:28:87$.

Catalyst Preparation. Catalysts were made by impregnating support materials in salt solutions. For single metallic Fe based catalysts, we used $Fe(NO_3)_3\cdot 9H_2O$/methanol solution or $Fe_2(SO_4)_3\cdot 5H_2O$ aqueous solution. Molar ratio of $Fe:Al_2O_3 = 1:16$ was used in preparing both catalyst systems. For bimetallic (Fe/Mo and Fe/Ru) catalysts, we used aqueous $Fe_2(SO_4)_3$ solutions and the molar ratios between reagents were kept at Fe: X(Mo or Ru): Al_2O_3 =1:0.17:16. When the $Al_2O_3-SiO_2$ hybrid support material was used in making the catalyst, the molar composition of the catalyst was Fe: Mo: SiO_2: $Al_2O_3 = 1:0.17:16:16$. The following outlines the detailed procedure for preparing an $Fe/Mo/Al_2O_3-SiO_2$ catalyst. Other catalysts were prepared using the same procedure except for different compounds. Support material (1 g) was suspended in 70 mL of water with stirring, followed by the addition of 0.020 g of $(NH_4)_6Mo_7O_{24}\cdot 4H_2O$ and 0.167 g of $Fe_2(SO_4)_3\cdot 5H_2O$. The mixture was stirred for 15 min and heated to 90 °C for 2 h while flowing a stream of N_2 over the mixture to remove the water. The material was then ground with an agate mortar to obtain a fine orange powder.

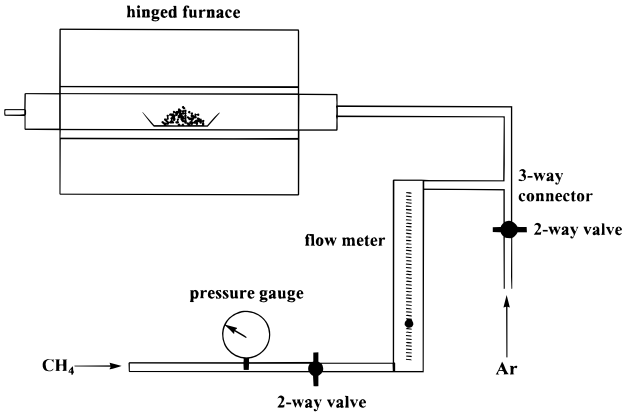

Figure 1. Schematic experimental setup for methane CVD synthesis of SWNTs. Typical growth temperature is 900 °C. The methane gas inlet pressure as measured by the gauge is 1.27 atm. Volume flow rate through the 1 in. quartz tube is ~6000 cm^3/min.

SWNT Synthesis. All the catalyst materials were calcined in air at 500 °C for 1 h, cooled to room temperature, and ground prior to CVD growth. Carbon nanotubes were synthesized by using the experimental setup shown in Figure 1. Typically, 0.1 g of the catalyst was placed into a quartz boat that was inserted into the center of a 1 in. diameter quartz tube mounted in an electric tube furnace. Ar was flown over the catalyst as it was heated from room temperature to 900 °C. The reaction began as Ar was replaced by CH_4 (flow rate 6000 cm^3/min) for the desired reaction time (2−45 min). The flow was then switched to Ar and the furnace was cooled to room temperature. When producing large quantities of SWNTs, we typically used 5.0 g of catalyst and the CVD reaction time was ~30 min.

Textural Property Characterization. Surface area and pore analysis of catalyst materials were performed by standard N_2 adsorption and desorption experiments using a Coulter SA-3100 surface area and pore analyzer. All catalysts were heated to 900 °C in Ar for 10 min prior to measurements in order to elucidate the textural properties of the catalysts at the beginning stage of the CVD growth. Surface areas were determined using the Brunauer−Emmett−Teller (BET) method.[30] Pore volumes were obtained at a normalized partial pressure (P_s/P_o) of 0.9814, and pore size distributions were calculated using the method of Barrett, Joyner, and Halenda (BJH).[31] All results are reported in accordance with the IUPAC recommendations for the interpretation of physisorption data. For instance, micropores are pores with diameters less than 2 nm, mesopores have diameters between 2 and 50 nm, and macropores have diameters greater than 50 nm.

Infrared Spectroscopy. DRFTIRS spectra were recorded using a Bruker Equinox 55 infrared spectrometer and a Spectra-Tech diffuse reflectance high-temperature chamber equipped with KBr windows. Support material or the metal loaded catalyst was ground to a fine powder with an agate mortar and placed on top of a powdered KBr layer (which served as the background) in the sample furnace. Samples for pyridine adsorption/desorption analysis were dehydrated in-situ by heating in a vacuum to 500 °C. After the samples were cooled to room temperature, pyridine vapor was introduced into the chamber by flowing Ar over the pyridine for 2 min, after which

the sample chamber was evacuated. Pyridine desorption studies were performed by collecting spectra as the samples were heated in steps to 500 °C under vacuum (2.0×10^{-3} Torr).

X-ray Photoemission Spectroscopy. X-ray photoelectron spectroscopy was performed using a Surface Science Instruments S−Probe, employing monochromated Al Kα (1.486 keV) as the source.

Characterization of Nanotube Materials. For all CVD grown samples, we first employed transmission electron microscopy (TEM) and scanning electron microscopy (SEM) to qualitatively estimate the yield of nanotubes. TEM was performed on a Phillips CM20 TEM operating at 200 kV. SEM was performed at 25 kV using a Hitachi H-800 field-emission instrument. Sample preparation for TEM involves sonicating the synthesized material in 1,2-dichloroethane for ∼10 min and placing a few drops of the resulting suspension onto holey carbon grids (Ted Pella, Inc.). To prepare samples for SEM, the synthesized materials were sonicated in 1,2-dichloroethane for 10 min, and a few drops of the suspension were placed onto a silicon substrate and allowed to evaporate. Samples were also prepared for SEM examination by placing the catalyst material onto a silicon substrate and performing nanotube growth using CH_4 CVD. For quantitative measurements, we carried out weight gain studies of the materials after CVD. Typically 0.1 g of catalyst material was first heated to 900 °C in flowing Ar, cooled to room temperature and weighed. The percent weight loss was calculated using the weight before and after heating in Ar. After CVD growth, the weight gain was calculated by using the known weight loss of the catalyst heated to 900 °C in Ar. We note that weight gain is a valid estimate of the yield of SWNTs only when the SWNTs are free of amorphous carbon coating and graphitic particles are absent in the CVD material, which is the case for the optimized SWNT materials in the current work.

3. Results and Disussion

Systematic Catalyst Optimization for SWNT Growth. In the initial methane CVD method, we used an $Fe(NO_3)_3/Al_2O_3$ catalyst prepared by impregnation in methanol and produced high quality individual SWNTs and a small fraction of bundled SWNTs.[25] The yield of SWNTs, however, is not sufficient for a bulk growth process where large quantities of SWNTs are desired. Also, a noticeable amount of graphitic particles exist in the material as byproducts. A number of steps were taken to systematically improve the yield of SWNTs.

Step 1: *Varying the Catalytic Metal-Bearing Compounds*. Different Fe-based salts were screened for improving the yield of SWNTs. We found that the $Fe_2(SO_4)_3/Al_2O_3$ prepared in an aqueous solution was superior to the $Fe(NO_3)_3/Al_2O_3$-based catalyst. A comparison of the TEM images of the SWNTs generated from the $Fe_2(SO_4)_3/Al_2O_3$ catalyst indicates the increased efficiency for SWNT growth compared with the $Fe(NO_3)_3/Al_2O_3$ system (Figure 2). Since SEM and TEM images are only qualitative in determining nanotube yield, weight gain results were used in correlation with microscopy data to quantify yield. Figure 3 shows the weight gain versus reaction time for a series of catalysts. The $Fe(NO_3)_3/Al_2O_3$ system initially has a steady growth rate, but levels off near 20 min, giving a 16 wt % gain after 45 min. The $Fe_2(SO_4)_3/Al_2O_3$ system has a higher initial growth rate but behaves similarly to the $Fe(NO_3)_3/Al_2O_3$ system giving a 21 wt. % yield after 45 min of CH_4 CVD. Upon closer inspection of the CVD material synthesized by the $Fe(NO_3)_3/Al_2O_3$ based catalyst using high magnification TEM, we detect the presence of graphitic particles with encapsulated metallic crystals inside (∼10 nm, data not shown). Their existence suggests that relatively large metal particles (∼10 nm) have formed in the CVD process due to weakly anchored metal species "lifting off" from the support material and sintering

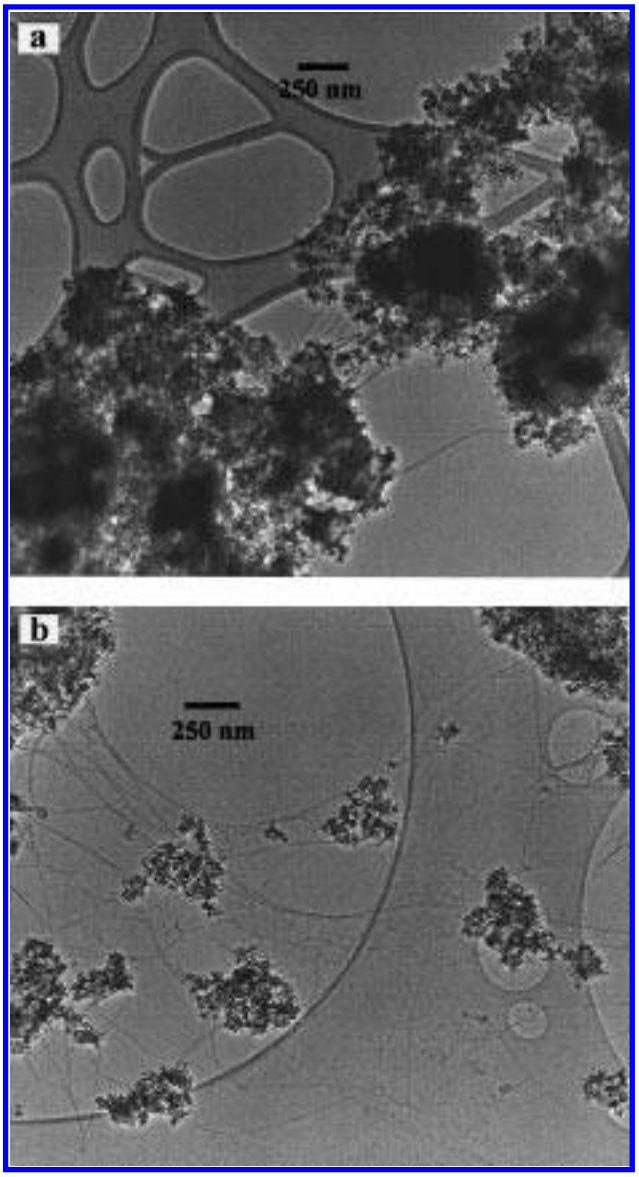

Figure 2. TEM images recorded with SWNT materials (a) made from the $Fe(NO_3)_3/Al_2O_3$-based catalyst after 10 min of CH_4 CVD and (b) made from $Fe_2(SO_4)_3/Al_2O_3$-based catalyst after 10 min of CH_4 CVD.

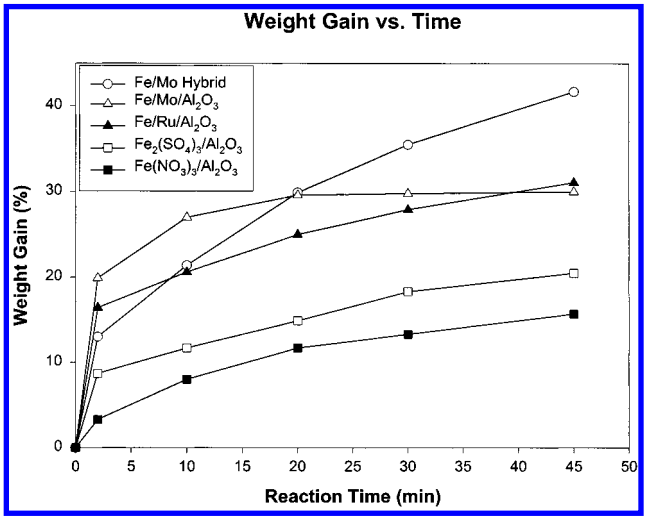

Figure 3. Weight gain vs time for a series of catalyst materials.

TABLE 1: Textural Properties of Catalysts after Heating to 900 °C in Ar

	catalysts heated to 900 °C in Ar					
support	$Fe(NO_3)/Al_2O_3$	$Fe_2(SO_4)_3/Al_2O_3$	Fe/Mo Al_2O_3	Fe/Ru Al_2O_3	Fe/Mo hybrid (1:1)	Fe/Mo hybrid (2.5:1)
surface area (m^2/g)	85	105	79	108	151	196
pore volume (mL/g)	0.19	0.89	0.61	0.59	0.71	0.79

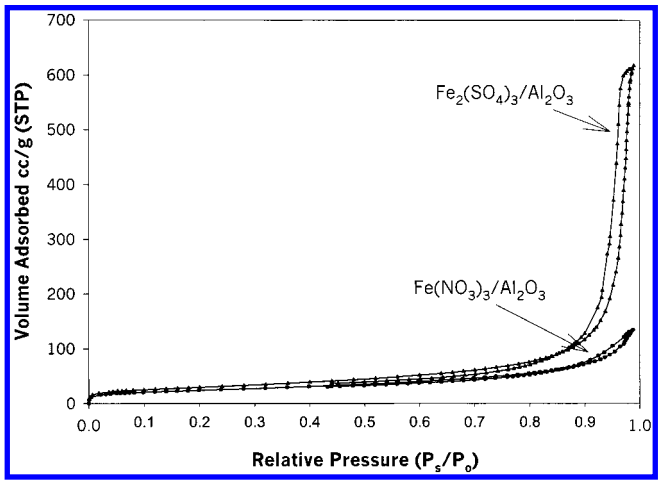

Figure 4. N_2 adsorption and desorption isotherms of catalyst materials after heating to 900 °C in Ar. The isotherm curves show a dramatic increase in mesopore volume (large absorption at $P_s/P_0 \sim 0.9$ in the upper curve) for the $Fe_2(SO_4)_3/Al_2O_3$-based catalyst over the $Fe(NO_3)_3/Al_2O_3$-based catalyst.

together. On the other hand, the CVD synthesized material using the $Fe_2(SO_4)_3/Al_2O_3$-based catalyst was nearly free of these unwanted graphitic structures. These results suggest that strong interactions exist between the metal species and the Al_2O_3 support for the $Fe_2(SO_4)_3$ derived catalyst, which contributes to the increased SWNT yield.

Different textural properties between the $Fe_2(SO_4)_3$- and $Fe(NO_3)_3$-derived catalysts provide further explanation to the observed difference in the yield of SWNTs for the two catalyst materials. Surface analysis has proven to be an excellent tool to probe the structures of catalyst materials. The pore structures of a catalyst could strongly influence the diffusion rates of molecular species and thus play important roles in determining the reaction kinetics. In Table 1, we show the textural properties of a series of catalysts after heating to 900 °C in Ar. We observe a dramatic increase in pore volume (0.89 vs 0.19 mL/g) and a slight increase in surface area (105 vs 85 m^2/g) for the $Fe_2(SO_4)_3/Al_2O_3$-based catalyst over the $Fe(NO_3)_3/Al_2O_3$-based catalyst (Figure 4). The large increase in pore volumes for the former could be attributed to two aspects. First, in an aqueous solution, strong interactions exist between sulfate ions and surface sites of alumina,[32,33] which allows the metal species to be uniformly dispersed and anchored on the alumina surface. This is advantageous because metal species can form active catalytic sites with high efficiency and density without being aggregated to form large particles. Second, the decomposition of $Fe_2(SO_4)_3$ to Fe_2O_3 occurs at $\sim$ 750 °C whereas the decomposition temperature is $\sim$ 140 °C for $Fe(NO_3)_3$. While a detailed understanding is required, we speculate that the decomposition of the highly dispersed and strongly anchored sulfate species at high temperature leads to the generation of the observed textural pores. In the CVD material synthesized by $Fe_2(SO_4)_3$-based catalyst, the absence of "lifted-off" metal particles and associated graphitic structures provides direct evidence for strong metal−support interactions. Thus, the increase in SWNT yield can be rationalized by better metal dispersion leading to higher density of catalytic sites and more open pore structures allowing efficient diffusion of reactant and product molecules in and out of the catalyst.

Step 2: *Bimetallic Catalysts.* Further increase in the yield of SWNTs was obtained by employing Fe/Mo and Fe/Ru catalysts after investigating various combinations of bimetallic catalyst materials. Figures 5 and 6 show SEM/TEM images of CVD materials synthesized by CH_4 CVD for 10 min at 900 °C using the $Fe/Mo/Al_2O_3$ and $Fe/Ru/Al_2O_3$ catalyst, respectively. In these materials, we observe more abundant SWNTs compared to the material produced by the $Fe_2(SO_4)_3/Al_2O_3$ catalyst. Results from weight gain experiments also show that the addition of Mo or Ru to the catalyst leads to a substantial increase in weight gain over the $Fe_2(SO_4)_3/Al_2O_3$ single-metal catalyst under identical reaction conditions (Figure 3), consistent with the qualitative TEM and SEM results. The $Fe/Mo/Al_2O_3$ catalyst led to a weight gain of 30% after 45 min of CH_4 CVD, and the $Fe/Ru/Al_2O_3$ catalyst showed a weight gain of 31% after 45 min of CVD. The $Fe/Mo/Al_2O_3$, $Fe/Ru/Al_2O_3$, and $Fe_2(SO_4)_3/Al_2O_3$ catalysts have similar textural structures as shown in Table 1, although we do observe the tendency of reduction in surface area and pore volume with the addition of Mo or Ru in the catalyst. Clearly, the increase in SWNT yield by the Mo or Ru addition cannot be accounted for by the textural properties of the three catalysts.

We tentatively attribute the increase in yield of SWNTs by the Fe/Mo catalyst to the roles played by Mo species in promoting the aromatization of methane at elevated temperatures. It has been established that supported Mo compounds on zeolite as well as transition alumina convert methane into aromatic species.[34] For the $Fe/Mo/Al_2O_3$ catalyst in our methane CVD process, it is plausible that intermediate aromatic hydrocarbons are generated on Mo sites. Owing to the close proximity between Mo and Fe catalytic sites where SWNT growth takes place, the intermediate aromatic species can feed into the SWNT growth sites with high efficiency, without being limited by diffusion.

The increase in SWNT yield due to the bimetallic Fe/Ru catalyst appears to have a different mechanism than that due to the Fe/Mo catalyst. We have observed an interesting and unique aspect of the CVD material synthesized by using the $Fe/Ru/Al_2O_3$ catalyst. That is, in the TEM, we observe abundant circular tubes (known as crop circles[35] as in laser ablation materials) and short tubes (0.1−2 μm in length) that are disconnected from the catalyst materials. These disconnected tubes appear to be grown in the gas phase, instead of grown off the catalyst particles or sonicated off the catalyst particles during TEM sample preparation. This is because for the CVD materials synthesized by $Fe/Mo/Al_2O_3$ catalysts, no appreciable disconnected tubes and circular tubes have been seen by TEM. Furthermore, the formation of disconnected tubes in the gas phase for the $Fe/Ru/Al_2O_3$ CVD system was confirmed by patterning silicon substrates with $Fe/Ru/Al_2O_3$ catalyst islands and characterizing the CVD grown nanotubes on the substrate by atomic force microscopy (AFM). Indeed, AFM imaging reveals nanotubes with both ends disconnected from the catalyst islands as well as circular tubes formed between the catalyst islands.[36] These results suggest that during the methane CVD process, metallic species are volatilized from the $Fe/Ru/Al_2O_3$

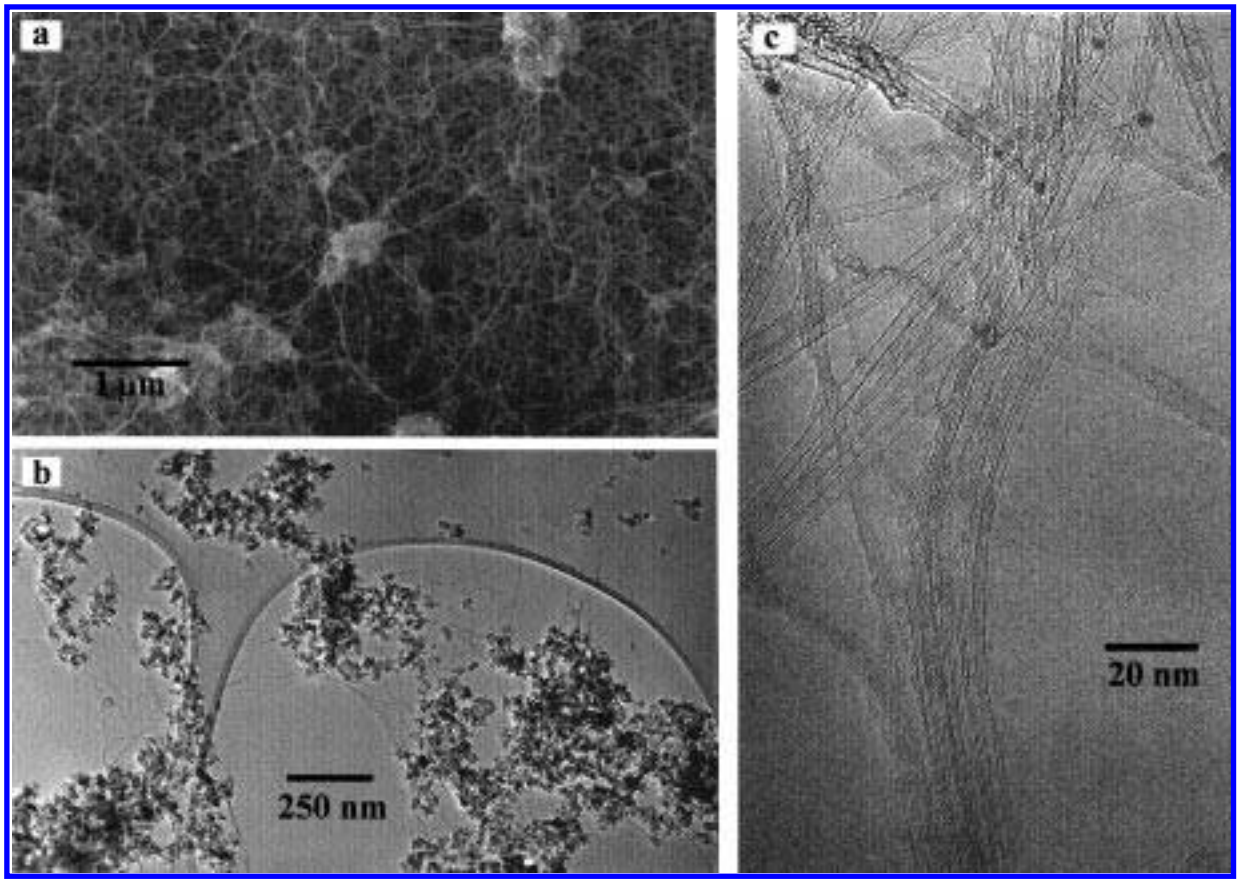

Figure 5. TEM micrographs of SWNT materials made from a bimetallic Fe/Mo/Al_2O_3 catalyst after 10 min CH_4 CVD. (a) Low magnification SEM, (b) low magnification TEM, and (c) high magnification TEM.

catalyst and catalyze the formation of nanotubes in the gas phase. Further experimental data and discussion of nanotube growth mechanism involving the Fe/Ru/Al_2O_3 catalyst are presented in a later section of this paper.

Step 3: *Varying the Support Material*. We have systematically investigated various support materials to further optimize the performance of the catalyst for the high yield synthesis of SWNTs. So far, we find that the best catalysts for producing high quality SWNTs using CH_4 CVD were made from an Fe/Mo catalyst supported on the $Al_2O_3-SiO_2$ hybrid support described in the Experimental Section. Figure 7 shows two TEM images of the synthesized nanotube material using the Fe/Mo/ hybrid catalyst. These low magnification images illustrate the remarkable abundance of nanotubes emanating from the catalyst particles, extending and forming a massive web. In Figure 8, we show a representative SEM image and high magnification TEM images. The SEM image (Figure 8a) clearly reveals the abundant fiberlike nanotube networks. The material is very uniform and has a consistent appearance throughout the sample under the SEM. High magnification TEM images (Figures 8b−d) reveal that the synthesized material consists of high quality individual and bundled single-walled nanotubes. At high magnification, the walls of the nanotubes are clearly resolved and show no amorphous carbon covering the nanotubes. The SWNTs are nearly perfect because they contain no sharp structural variations due to topological defects along their axes, only buckling and smooth bending of the nanotubes are seen due to nanotube entanglement. Quite often, ends (Figure 8c) as well as end-on views of nanotube bundles (Figure 8d) are observed. By measuring over 100 SWNTs, we find that SWNTs have diameters dispersed in the range of 0.7−5 nm with a peak diameter close to 1.7 nm. Occasionally, we also detect the presence of double walled nanotubes, but they are essentially negligible relative to the abundant SWNTs. Importantly, we observe nearly no graphitic particles due to lifted-off metal particles or amorphous carbon particles due to pyrolysis and buildup. Weight gain measurements with the Fe/Mo/hybrid catalyst for 45 min approaches 45 wt %, which is the highest among all catalysts studied in the current work. These results show that the methane CVD SWNT materials are of comparable quality and purity to those obtained by laser ablation and arc discharge, which is very significant because the CVD approach has the potential to be scaled up for the production of large quantities of perfect nanotube materials. For instance, starting with 5 g of the Fe/Mo/hybrid catalyst, we synthesized ∼1.5 g of SWNTs by methane CVD in 30 min.

The increase in SWNT yield with the Fe/Mo/hybrid catalyst can be at least partly attributed to its more open textural structure compared to the Fe/Mo/Al_2O_3 catalyst. As shown in Table 1 and Figure 9, the Fe/Mo/hybrid catalyst exhibits the highest surface area and largest pore volume among all the catalysts investigated in the current work. The large pore volume consists of a large fraction of mesopores (Figure 9) that allow efficient diffusion of reactant and intermediate hydrocarbon species, which could be responsible for efficient SWNT growth and high yield. To understand the textural properties of the $Al_2O_3-SiO_2$ hybrid support and the catalyst at a microscopic level, we have carried out IR spectroscopy (see the next subsection) and TEM studies. Both studies found that the silica phase in the catalyst does not conform as uniform layers on the alumina surface. We found by TEM that the silica phase partially covers and interconnects the alumina particles. Therefore, the silica particles effectively act as "spacers" that prevent the catalyst material from sintering and collapsing, which provides a rationale for a

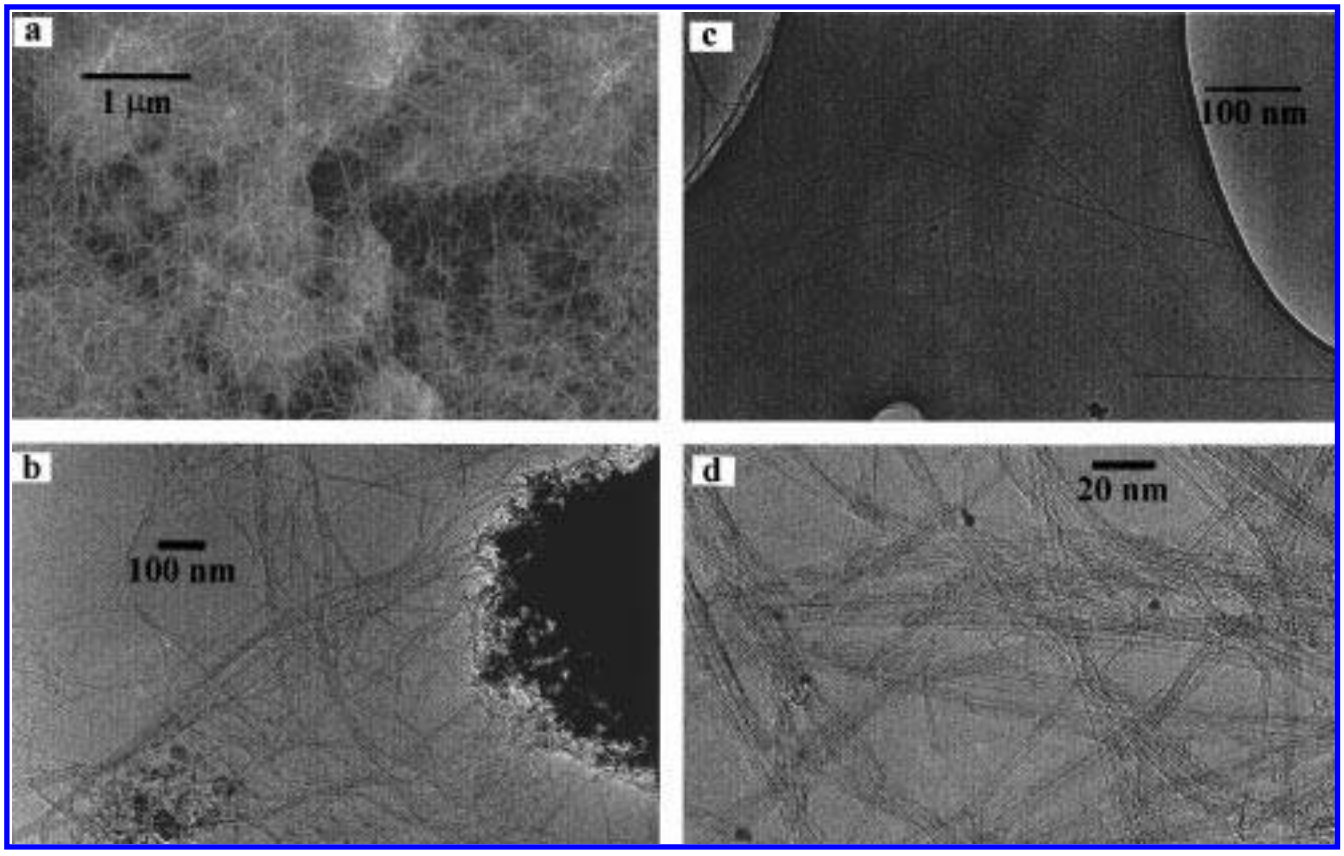

Figure 6. TEM micrographs of SWNT materials made from a bimetallic Fe/Ru/Al_2O_3 catalyst after 10 min of CH_4 CVD. (a) Low magnification SEM, (b) low magnification TEM, (c) intermediate, and (d) high magnification TEM.

highly open pore structure of the support and the catalyst. To reduce sintering, the silica phase must be thermally stable at elevated temperatures and is achieved by our sol−gel process using HF as the gel-forming catalytic agent. Hybrid materials obtained using other types of acid or base all exhibit poor textural properties at high temperatures and are inferior for CVD SWNT growth. Si−F is known as one of the strongest chemical bonds and remains intact up to ∼2000 °C. Furthermore, sol−gel chemistry has established the displacement of −OH groups on the silica surface by F^- to give Si−F groups, which leads to less water content and enhances the thermal stability of the silica structure.[37−39] We indeed confirmed the presence of F in the hybrid based catalyst after heating to 900 °C by XPS. A peak positioned at 686 eV was observed corresponding to F (1s) in the XPS spectrum. The idea of using silica phase to improve textural properties and reduce sintering of catalysts has been used previously in catalytic reactions. For instance, Miller et al. have reported improved textural and catalytic properties of ZrO_2/silica catalyst over pure ZrO_2 catalyst for the 1-butene isomerization reactions.[40]

The Nature of Support Materials. We have systematically investigated various silica, alumina and multicomponent silica−alumina supported catalysts for the methane CVD process throughout this work. A general conclusion is reached that silica supported catalysts are inferior to alumina based catalysts for synthesizing high yield and purity bulk SWNT materials, even when the catalysts have similar textural properties. For instance, we prepared a pure silica support in the same manner as the hybrid support described above without the presence of Al_2O_3. The catalyst based on the pure silica material exhibits similar surface area and pore volume as the Fe/Mo/Al_2O_3 and the Fe/Mo/hybrid catalysts. As found by TEM and weight gain studies, the CVD material made by the silica based catalyst led to much lower yield and purity SWNTs than the materials obtained by the Fe/Mo/Al_2O_3 and Fe/Mo/hybrid catalysts. Graphitic particles with enclosed metal nanocrystals were frequently observed in the synthesized material, indicating weaker metal−support interactions on silica supports than on alumina and the hybrid supports. This led us to investigate the surface chemistry aspects of the support materials.

In Figure 10a, we show DRFTIRS spectra of hydroxyl groups on the surfaces of alumina, silica and the hybrid material. The spectra were recorded at room temperature after removing physisorbed water by heating the samples to 500 °C in a vacuum (1×10^{-3} Torr) for 0.5 h. The pure alumina material was found to exhibit several types of hydroxyl groups in the range of 3400−3750 cm^{-1},[41−43] while the silica shows a peak at 3746 cm^{-1} corresponding to terminal hydroxyl groups.[44] The spectrum in the −OH regime for the hybrid material qualitatively resembles the sum of the spectra of Al_2O_3 and silica. Pyridine adsorption−desorption studies on silica found only weakly H-bonded pyridine to surface hydroxyls (peaks at 1447 and 1597 cm^{-1}, diminished upon heating to 150 °C; data not shown).[44] Al_2O_3 exhibits Lewis acidity as shown in Figure 10b, where two peaks (1454 and 1615 cm^{-1}) corresponding to Lewis-coordinated pyridine persist up to 500 °C.[43−45] Figure 10c shows pyridine desorption results for the hybrid support that exhibit strong Lewis acidity (persistent peaks at 1492, 1597, and 1622 cm^{-1}) and some Brönsted acidity (peaks centered at 1549 and 1640 cm^{-1}). The Lewis acidity of the hybrid material is stronger than that of alumina as evidenced by the more persistent Lewis-coordinated pyridine peaks upon heating to high temperatures. We attribute this enhanced acidity to the inductive effects of Si−F groups in the hybrid material.[44] On the other hand, the Brönsted acidity of the hybrid could be due to strongly H-bonded H_2O molecules or trapped HF molecules.

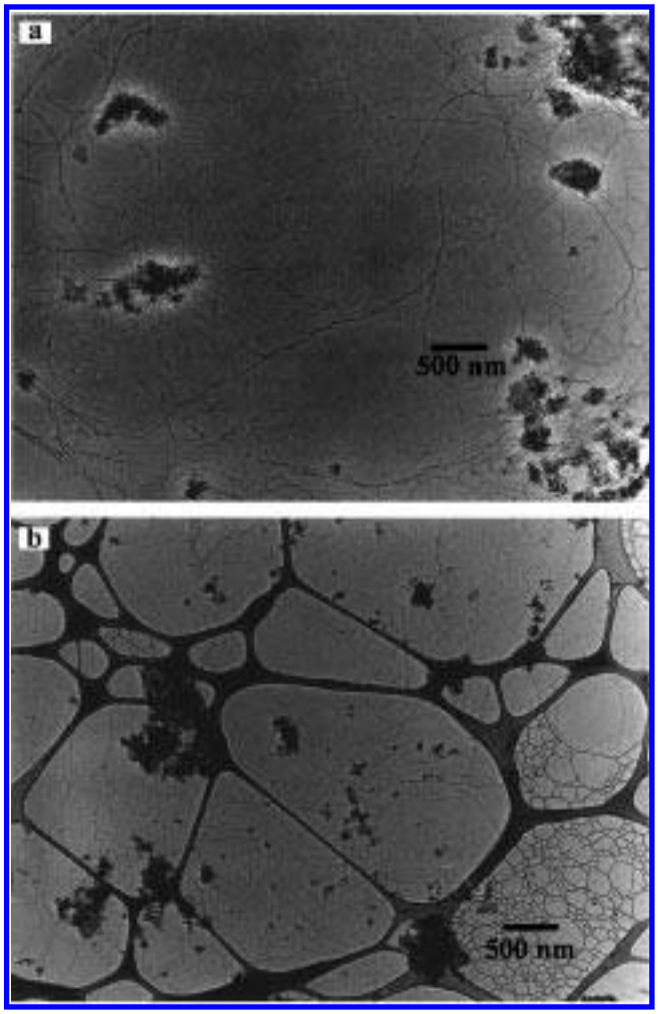

Figure 7. Low magnification TEM images of SWNT materials synthesized by CH_4 CVD in 10 min using the Fe/Mo/hybrid catalyst. a and b are images recorded with samples obtained by different CVD runs, showing the high reproducibility of the synthesis process.

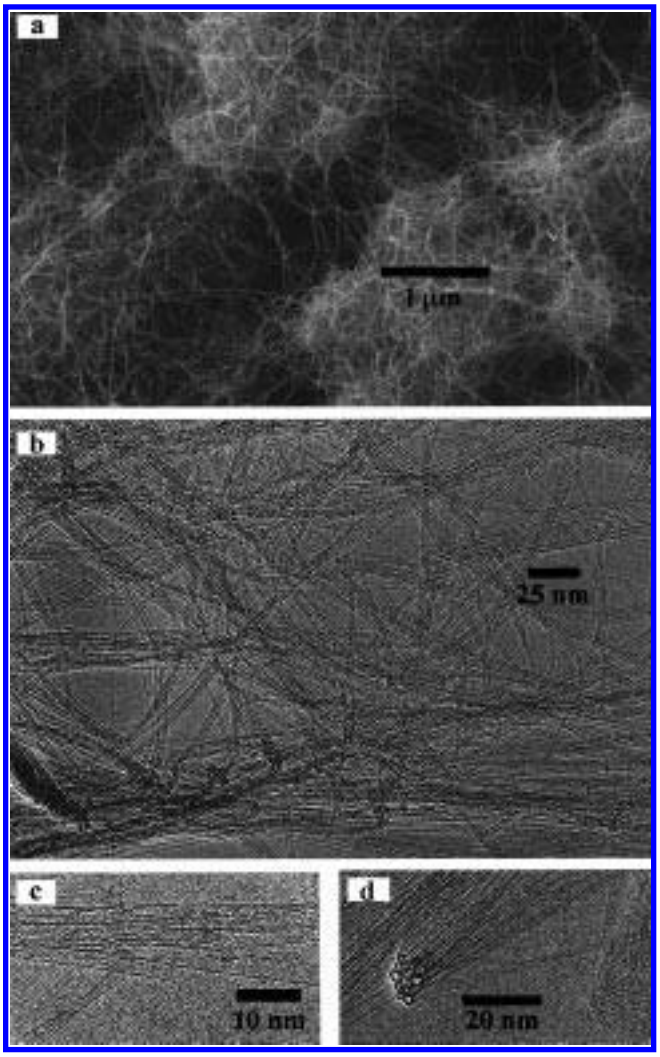

Figure 8. (a) SEM and (b−d) high magnification TEM images of SWNT materials synthesized using the Fe/Mo/hybrid catalyst.

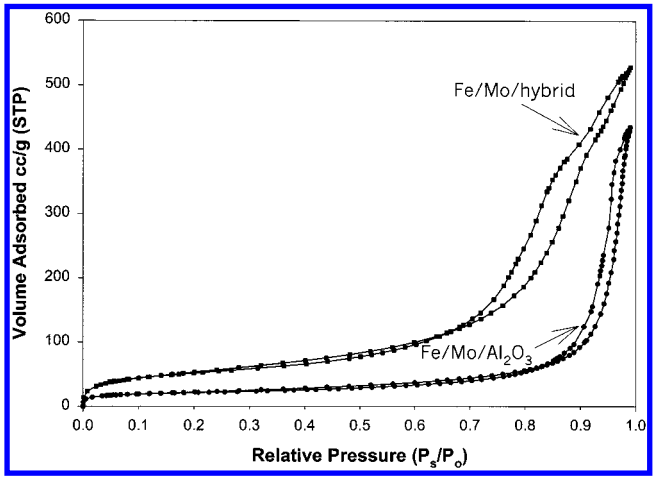

Figure 9. N_2 adsorption and desorption isotherms of Fe/Mo/Al_2O_3 and Fe/Mo/hybrid catalysts after heating to 900 °C in Ar. The Fe/Mo/hybrid catalyst exhibits higher surface area (higher adsorbed volume at $P_s/P_0 \sim 0.05$) and larger mesopore volume (higher adsorbed volume at $P_s/P_0 \sim 1$) than those of the Fe/Mo/Al_2O_3 catalyst.

The IR results presented above have several implications. First, it is confirmed that the alumina is not fully covered by the silica phase in the hybrid support material, and the silica phase is merely interconnecting the alumina particles. This is consistent with our proposal that the hybrid support leads to a better performing catalyst due to reduced sintering by the silica "spacers". Second, since both the alumina and hybrid support lead to excellent catalysts for CVD growth of SWNTs, and the hybrid support has highly accessible alumina surface sites, we conclude that alumina is in general better than silica as catalyst support for the methane CVD process. A main reason seems to be that metal−support interactions are weaker on silica supports than on alumina supports, as found by the TEM observation of metal particle lift-off in silica supported catalysts after CVD. The strong metal−support interaction between alumina surface sites and $Fe_2(SO_4)_3$ can be attributed to chemical reactions that occur in the impregnation step.[32,33] However, it is not clear at the present time if the Lewis acid sites on the alumina surface are directly involved in reactions with methane via heterolytic cleavage,[46] affording a more active catalyst material. This issue will be investigated in future studies.

SWNT Growth Mechanism and Rate. In the SWNT materials synthesized by $Fe_2(SO_4)_3/Al_2O_3$, Fe/Mo/Al_2O_3 and Fe/Mo/hybrid catalysts, we frequently observed closed SWNT ends that are free of encapsulated metal particles, far away from the catalyst support materials (Figure 11a, left part Figure 8c). This strongly suggests that the SWNTs are formed predominantly through the "base growth" mechanism in the methane CVD process. That is, during the CVD process, the catalyst particles responsible for nanotube nucleation and growth remain pinned on the support surface.[25,26,47−49] However, in the CVD materials

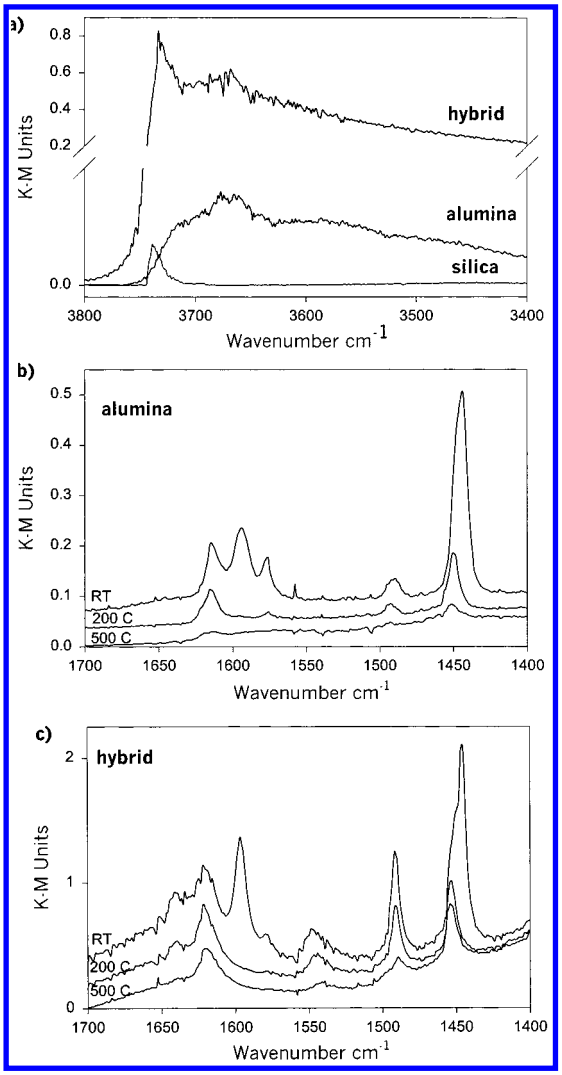

Figure 10. DRFTIRS of catalyst support materials. (a) Spectra of Al_2O_3, silica, and the $Al_2O_3-SiO_2$ hybrid material in the −OH stretching region. (b) Results of pyridine desorption experiments on the Al_2O_3 surface. (c) Results of pyridine desorption studies of the $Al_2O_3-SiO_2$ hybrid.

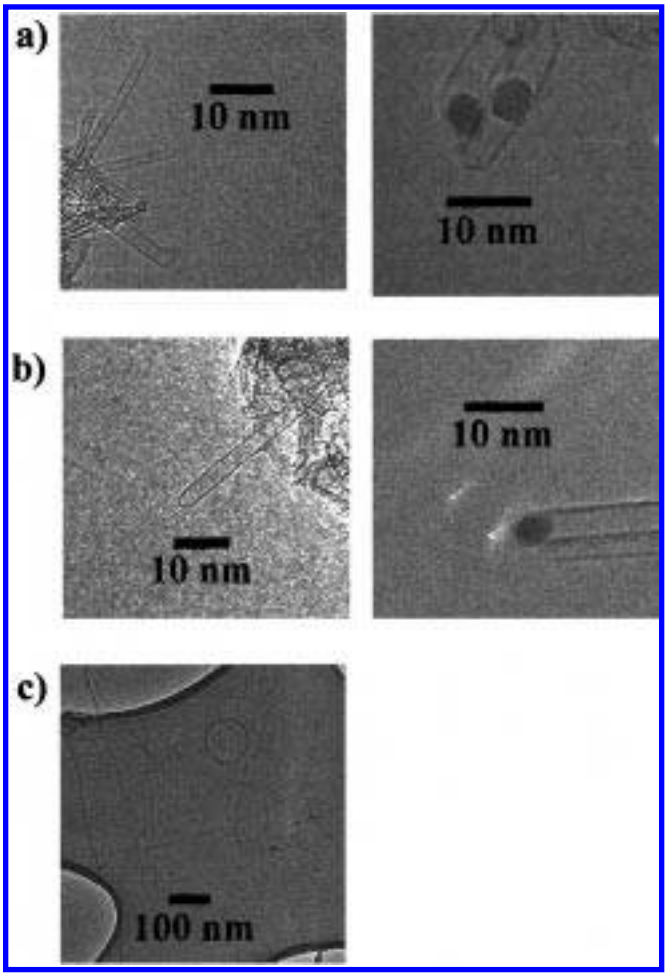

Figure 11. TEM images of SWNTs. (a) Left part: high-resolution image showing closed nanotube ends in the CVD material synthesized from the Fe/Mo/hybrid catalyst. Right part: a small fraction of SWNTs contain metal particles at their ends in the same material. (b) High-resolution TEM images of nanotubes in the materials synthesized from the $Fe/Ru/Al_2O_3$ catalyst. Left part: a SWNT with closed end. Right part: a SWNT with metal particle at the end. (c) Disconnected and circular tubes in the CVD material synthesized by using the $Fe/Ru/Al_2O_3$ catalyst.

synthesized from the bimetallic $Fe/Mo/Al_2O_3$ and Fe/Mo/hybrid catalysts, we also noticed a small fraction (∼5%) of SWNTs that do contain metal particles at their ends (Figure 11a, right part). This indicates tip-growth as the secondary nanotube growth mechanism in methane CVD using the Fe/Mo catalysts. Similarly, in the CVD material obtained by the $Fe/Ru/Al_2O_3$ catalyst, the majority of the nanotube ends were found closed and metal-particle free (Figure 11b, right part), while a small fraction of metal containing SWNT ends was observed (Figure 11b, lower part). Also, we frequently observed crop circles as well as "disconnected" nanotubes (Figures 11c and 6c) in the CVD material derived from the $Fe/Ru/Al_2O_3$ catalyst, which indicates that a gas-phase nanotube growth mechanism operates in this system. We propose that volatilized Ru species are responsible for catalyzing the formation of the disconnected and circular nanotubes. From the Fe−Ru binary phase diagram[50] and due to the small-size effect, it is possible that the Ru nanophase in the Fe−Ru mixture exhibits a low melting temperature (∼1000 °C) and sufficient vapor pressure. Detailed mechanisms for the metal vaporization and the subsequent gas phase nanotube formation are currently lacking. Nevertheless, we did confirm the activity of Ru species in catalytic growth of SWNTs. We prepared a Ru/Al_2O_3 catalyst and found that the Ru catalyst indeed led to SWNTs in the methane CVD process.[51]

An obvious feature in the weight gain data for all catalyst systems is the decrease in growth rate with time (Figure 3). That is, the weight gain deviates from a linear relationship with time and levels off after only a few minutes of CVD reactions. This phenomenon seems to be common in the CVD growth of nanotubes. For instance, in our recent work of growing regular arrays of aligned multiwalled nanotubes on porous silicon substrates, the nanotube length as a function of time was found to deviate from a straight line after ∼20−30 min of CVD reaction.[13] In the growth of SWNTs using ethylene as carbon feedstock, the growth rate was also found to decrease at long reaction times and was attributed to the thickening mat of nanotubes.[28] We believe that at least one of the rate-limiting steps in CVD is gas diffusion. Comparing the weight gain curves in Figure 3 obtained with various catalysts and correlating them with the textural properties of the catalysts in Table 1, we do observe the trend that a catalyst exhibiting more open pore structures (larger pore volume) improves the nanotube growth rate and yield (weight gain). These results strongly suggest the importance of highly porous catalysts for CVD nanotube synthesis. A detailed mechanism is lacking to account for the

growth rate decrease and termination at long reaction times. However, we believe that plausible possibilities include pore clogging and catalyst poisoning by the grown nanotubes and small amounts of deposited amorphous carbon.

4. Conclusion and Future Direction

The synthesis of bulk amounts of high quality single-walled carbon nanotubes (SWNTs) is accomplished by systematically optimizing the chemical compositions and textural properties of catalysts within the methane CVD synthetic approach. Materials that contain ~42 wt % of SWNTs are obtained by CVD and scale-up to the gram level has been demonstrated. The nanotube materials consist of individual and bundled SWNTs that are nearly free of defects and amorphous carbon coating on the nanotube walls.

We have taken significant steps to understand the catalyst materials and the CVD process. The key to the synthesis of high yield, quality, and purity SWNTs is found to be the catalyst material. Iron sulfate is found to interact strongly with the surface of alumina support, which leads to high metal dispersion, virtually eliminates metal lift-off and aggregation and produces textural mesopores. In terms of chemical compositions, the Fe/Mo bimetallic catalyst increases SWNT yield over Fe catalysts possibly by promoting aromatization reactions of methane. The Fe/Ru bimetallic catalyst also leads to higher yield of SWNTs through the formation of circular tubes and "free-floating" tubes in the gas phase. Alumina is found to be a superior catalyst support material over silica partly due to stronger metal−support interactions on the alumina. A novel $Al_2O_3-SiO_2$ hybrid support material is synthesized by sol−gel to further increase the yield of SWNTs. The alumina phase in the hybrid support retains its chemical characteristics without being fully covered by the silica phase. The advantages of the hybrid support over the pure alumina support include higher surface-area and larger pore volume at elevated temperatures due to the silica "spacing effect".

There is still significant room for future work to optimize methane CVD SWNT synthesis and understand the processes involved in the catalysis of C_1 to C_∞. In terms of SWNT yield optimization, future work should include rational design and creation of new types of catalyst support materials and catalysts. An ideal catalyst should exhibit the desired textural properties that are stable at elevated temperatures in order to obtain high densities of catalytic sites and enable efficient and steady nanotube growth. For instance, a catalyst based on an alumina support that exhibits several level of pore structures (e.g., 1 nm scale and 1−10 μm scale) will allow efficient catalyst particle formations and "free" space for gas diffusion and nanotube growth. In terms of the chemistry aspects of catalyst materials and CVD processes, detailed understanding should be obtained on the microscopic catalyst structures, metal−support interactions and mechanisms of nanotube growth, kinetics, and termination. Further understanding and optimization could enable the synthesis of 10 g of SWNTs by 1 g of catalyst by CVD.

Acknowledgment. This work is supported by National Science Foundation (NSF Grant ECS-9871947), the Semiconductor Research Corporation (SRC Grant 98-MJ-630), the Camille Henry Dreyfus Fondation, and the American Chemical Society.

References and Notes

(1) Iijima, S. *Nature* **1991**, *354*, 56.
(2) Dresselhaus, M. S.; Dresselhaus, G.; Eklund, P. C. *Science of Fullerenes and Carbon Nanotubes*; Academic Press: San Diego, 1996.
(3) Yakobson, B. I.; Smalley, R. E. *Am. Sci*. **1997**, *85*, 324.
(4) Ebbesen, T. W. *Phys. Today* **1996**, *49*, 26.
(5) Dai, H. J.; Hafner, J. H.; Rinzler, A. G.; Colbert, D. T.; Smalley, R. E. *Nature* **1996**, *384*, 147.
(6) Dai, H.; Franklin, N.; Han, J. *Appl. Phys. Lett*. **1998**, *73*, 1508.
(7) Wong, S.; Harper, J.; Lansbury, P.; Lieber, C. M. *J. Am. Chem. Soc*. **1998**, *120*, 603.
(8) Wong, S.; Joselevich, E.; Woolley, A.; Cheung, C.; Lieber, C. *Nature* **1998**, *394*, 52.
(9) Rinzler, A. G.; Hafner, J. H.; Nikolaev, P.; Lou, L.; Kim, S. G.; Tomanek, D.; Nordlander, P.; Colbert, D. T.; Smalley, R. E. *Science* **1995**, *269*, 1550.
(10) de Heer, W. A.; Chatelain, A.; Ugarte, D. *Science* **1995**, *270*, 1179.
(11) Saito, Y.; Hamaguchi, K.; Hata, K.; Tohji, K. *Ultramicroscopy* **1998**, *73*, 1.
(12) Wang, Q.; Setlur, A.; Lauerhaas, J.; Dai, J.; Chang, R. H. *Appl. Phys. Lett*. **1998**, *72*, 2912.
(13) Fan, S.; Chapline, M.; Franklin, N.; Tombler, T.; Cassell, A.; Dai, H. *Science* **1999**, *283*, 512.
(14) Tans, S.; Verschueren, A.; Dekker: C. *Nature* **1998**, *393*, 49.
(15) Martel, R.; Schmidt, T.; Shea, H. R.; Hertel, T.; Avouris, P. *Appl. Phys. Lett*. **1998**, *73*, 2447.
(16) Soh, H.; Morpurgo, A.; Kong, J.; Marcus, C.; Quate, C.; Dai, H. *Appl. Phys. Lett*. **1999**. Submitted for publication.
(17) Bethune, D. S.; Kiang, C. H.; DeVries, M.; Gorman, G.; Savoy, R.; Vazquez, J.; Beyers, R. *Nature* **1993**, *363*, 605.
(18) Journet, C.; Maser, W. K.; Bernier, P.; Loiseau, A.; Delachapelle, M. L.; Lefrant, S.; Deniard, P.; Lee, R.; Fischer, J. E. *Nature* **1997**, *388*, 756.
(19) Thess, A.; Lee, R.; Nikolaev, P.; Dai, H. J.; Petit, P.; Robert, J.; Xu, C. H.; Lee, Y. H.; Kim, S. G.; Rinzler, A. G.; Colbert, D. T.; Scuseria, G. E.; Tomanek, D.; Fischer, J. E.; Smalley, R. E. *Science* **1996**, *273*, 483.
(20) Tibbetts, G. G. In *Carbon Fibers, Filaments and Composites*; Kluwer Academic: Amsterdam, 1990; pp 73−94.
(21) Tibbetts, G. G. *Appl. Phys. Lett*. **1983**, *42*, 666.
(22) Endo, M. *Chemtech* **1988**, 568−576.
(23) Snyder, C. E.; Mandeville, W. H.; Tennent, H. G.; Truesdale, L. K. US Patent, 1989.
(24) Baker, R. T. K.; Rodriguez, N. M. In *Symposium of the Materials Research Society*; Materials Research Society: 1994; Vol. 349, p 251.
(25) Kong, J.; Cassell, A. M.; Dai, H. *Chem. Phys. Lett*. **1998**, *292*, 567.
(26) Kong, J.; Soh, H.; Cassell, A.; Quate, C. F.; Dai, H. *Nature* **1998**, *395*, 878.
(27) Cheng, H.; Li, F.; Su, G.; Pan, H.; Dresselhaus, M. *Appl. Phys. Lett*. **1998**, *72*, 3282.
(28) Hafner, J.; Bronikowski, M.; Azamian, B.; Nikolaev, P.; Colbert, D.; Smalley, R. *Chem. Phys. Lett*. **1998**, *296*, 195.
(29) Flahaut, E.; Govindaraj, A.; Peigney, A.; Laurent, C.; Rao, C. N. *Chem. Phys. Lett*. **1999**, *300*, 236.
(30) Brunnauer, S.; Emmett, P.; Teller, E. *J. Am. Chem. Soc*. **1938**, *60*, 309.
(31) Barrett, E.; Joyner, L.; Halenda, P. *J. Am. Chem. Soc*. **1951**, *73*, 373.
(32) Rajan, S. S. S. *Soil Sci. Soc. Am. J*. **1978**, *42*, 39.
(33) Okamoto, Y.; Imanaka, T. *J. Phys. Chem*. **1988**, *92*, 7102.
(34) Wang, L.; Tao, L.; Xie, M.; Xu, G. *Catal. Lett*. **1993**, *21*, 35.
(35) Liu, J.; Dai, H. J.; Hafner, J. H.; Colbert, D. T.; Smalley, R. E.; Tans, S. J.; Dekker: C. *Nature* **1997**, *385*, 780.
(36) Kong, J.; Dai, H. Unpublished results.
(37) Brinker, C. J.; Scherer, G. W. *Sol−Gel Science*: *The Physics and Chemistry of Sol−Gel Processing*; Academic Press: San Diego, 1990.
(38) Nassau, K.; Rabinovich, E.; Miller, A.; Gallagher, P. *J. Non-Cryst. Solids* **1986**, *82*, 78.
(39) Winter, W.; Chan, J.; Frattini, R.; Jonas, J. *J. Noncryst. Solids* **1988**, *105*, 214.
(40) Miller, J.; Rankin, S.; Ko, E. *J. Catal*. **1994**, *148*, 673.
(41) Morterra, C.; Magnacca, G. *Catal. Today* **1996**, *27*, 497.
(42) Tsyganenko, A.; Mardilovich, P. *J. Chem. Soc., Faraday Trans*. **1996**, *92*, 4843.
(43) Liu, X.; Truitt, R. *J. Am. Chem. Soc*. **1998**, *119*, 99856.
(44) Hair, M. L. *Infrared Spectroscopy in Surface Chemistry*; Marcel Dekker: New York, 1967.
(45) Parry, E. *J. Catal*. **1963**, *2*, 371.
(46) Schobert, H. *The Chemistry of Hydrocarbon Fuels*; Butterworth & Co.: Boston, 1990.
(47) Baker, R. T. K. *Carbon* **1989**, *27*, 315.
(48) Tibbetts, G. G.; Devour, M. G.; Rodda, E. J. *Carbon* **1987**, *25*, 367.
(49) Amelinckx, S.; Bernaerts, D.; Zhang, X. B.; Van Tendeloo, G.; Van Landuyt, J. *Science* **1995**, *267*, 1334.
(50) Massalski, T. B. *Binary Alloy Phase Diagrams*; William W. Scott, Jr., Ed.; American Society for Metals: Metals Park, OH, 1990.
(51) Cassell, A.; Dai, H. Unpublished results.